Available online at www.sciencedirect.com
ScienceDirect
Thermochimica Acta 455 (2007) 2–6
thermochimica acta
www.elsevier.com/locate/tca

Specific heat of a $YCrO_3$ single crystal as investigated by a Si–N membrane based microcalorimeter

J.W. Kim, Y.S. Oh, K.S. Suh, Y.D. Park, Kee Hoon Kim *

CSCMR and FPRD, School of Physics and Astronomy, Seoul National University, Seoul 151-747, Republic of Korea

Available online 10 December 2006

Abstract

We report the specific heat measurement of a $YCrO_3$ single crystal in a wide temperature range from 30 to 360 K by use of a newly designed microcalorimeter with high sensitivity about ∼1 μJ/K. The measured heat capacity data exhibit a λ-like shape at the Néel temperature $T_N \approx 140$ K as consistent with the second order magnetic transition. When the phonon specific heat is subtracted by use of that of a non-magnetic analogue $LaGaO_3$ with an orthorhombic structure, the remaining entropy is much higher than the expected magnetic entropy from Cr^{3+} ($S = 3/2$) ions. We attribute the excess entropy to the additional phonon entropy caused by the monoclinic structure of $YCrO_3$, which can be intimately related to its ferroelectric property.

Keywords: Heat capacity; Silicon nitride membrane; $YCrO_3$; Multiferroic

1. Introduction

Multiferroic materials wherein multiple ferroic orders such as ferroelectricity and antiferromagnetism can coexist and be coupled to each other, have drawn renewed attention in recent years [1–3]. While scientific motivation to understand the generation and the coupling mechanisms of the multiple ferroic orders is quite interesting by itself, the material system has also promising application potentials for a new multifunctional memory device. Among many candidate compounds, Bi-doped perovskites such as $BiMnO_3$ [4,5], $BiFeO_3$ [6], and $BiCrO_3$ [7] are reported to exhibit the coexistence of the low temperature magnetic transitions around ∼100 K and high temperature ferroelectricity above room temperature. The latter is known to be driven by the peculiar electronic states of Bi^{3+} that has the $6s^2$ lone pair [8]. On the other hand, non-Bi-doped materials such as $YMnO_3$ shows an improper ferroelectricity driven by its structural geometry, *i.e.*, ferroelectricity is a secondary order parameter driven by its hexagonal structure [9]. In addition, emerging materials such as $TbMnO_3$ and $Ni_3V_2O_8$ are known to exhibit the improper ferroelectricity driven by their non-collinear magnetic ordering that breaks both inversion and time-reversal symmetry [10].

Perovskite chromite is yet another interesting system in which researchers are looking for an evidence of multiferroic orders. In particular, Serrao et al. [11] have recently reported that a polycrystalline $YCrO_3$ sample exhibits evidences of bi-ferroicity; dielectric constant has a frequency dependent peak around the ferroelectric Curie–Weiss temperature $T_C \approx 473$ K and magnetic susceptibility shows a sharp increase at the canted antiferromagnetic (AFM) transition $T_N = 140$ K. However, contrary to the other perovskite system, still unknown is the evidence of ferroelectricity in a single crystal and its mechanism. To better investigate the occurrence and the origin of the possible ferroelectricity, we have grown a $YCrO_3$ single crystal through the flux melting method [12] and have been investigating its specific heat properties. However, our initial attempt to use a conventional calorimeter made of the sapphire platform (from Quantum Design) has failed because the sample heat capacity is too small to be detected due to the limited sample size (<100 μg) and the large addenda heat capacity.

Herein, we report the first specific heat measurement of a $YCrO_3$ single crystal with its mass 55 μg using a newly designed microcalorimeter based on the Si–N membrane. We have recently proved that the new microcalorimeter is especially suitable for an accurate specific heat measurement of such a tiny crystal [13]. We have also developed the so-called curve fitting method (CFM) to accurately determine specific heat of the specimen.

* Corresponding author. Tel.: +82 2 880 9068; fax: +82 2 880 0769.
E-mail address: khkim@phya.snu.ac.kr (K.H. Kim).

0040-6031/$ – see front matter © 2006 Elsevier B.V. All rights reserved.
doi:10.1016/j.tca.2006.12.007

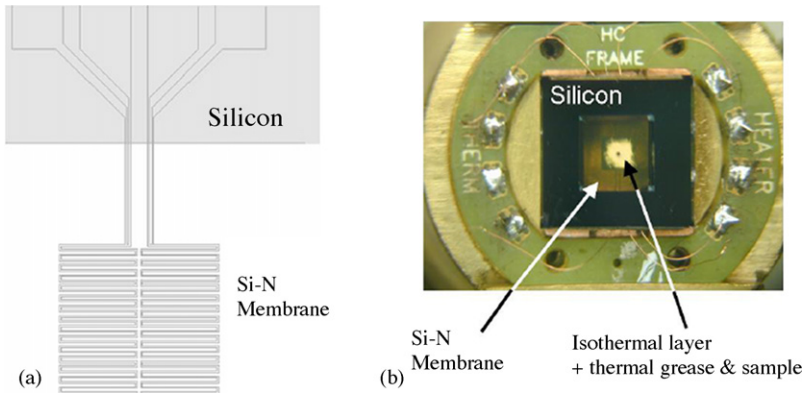

Fig. 1. (a) A schematic diagram of the microcalorimeter used in this study. The heater/sensor region is well confined [13]. (b) A photograph of the microcalorimeter installed on a commercial heat capacity puck (PPMS^{TM}, Quantum Design). A piece of $YCrO_3$ single crystal with its mass 55 μg (a black dot in the center) and a white grease (a white region in the center) are mounted on top of the isothermal layer (a square inside the semi-transparent membrane).

2. Experimental

2.1. Microcalorimeter and sample preparations

Among various efforts to measure sensitively the specific heat of a sample with mesoscopic length scale, a novel membrane microcalorimeter fabricated by the semiconductor lithographic techniques has provided a new breakthrough to achieve extremely small addenda heat capacity down to ∼nJ/K [14–17]. With this breakthrough, the microcalorimeter is being increasingly used to measure various mesoscopic samples with greatly enhanced sensitivity. A few examples include sub-angstrom thick metallic films, nano-liters of organic liquids, nano-grams of polymers and micrometer sized bio-materials [18–21].

We have recently developed a new type microcalorimeter based on a Si–N membrane for measuring specific heat of a small single crystal or films in a wide temperature range and under high magnetic fields. In particular, with the new heater/sensor design as shown in Fig. 1(a), we have reproduced the standard specific heat data of Cu (∼0.3 mg) within 5% between 30 and 360 K, of which results will be published elsewhere.

We have grown a single crystal of $YCrO_3$ with its mass 55 μg by the flux melting method in a Pt crucible by use of the $PbO–PbF_2–B_2O_3$ flux [12]. The Pt crucible with the flux and stoichiometric powders was kept at 1260 °C for 12 h and slowly cooled by 1 K/h until 950 °C to be subsequently cooled down to room temperature by 120 K/h. The crystal axis of the grown crystal was identified by a Laue camera and a conventional X-ray diffractometer. However, we could not distinguish the space group of the small crystal with those measurements only. To confirm a magnetic transition of the sample, we measured the magnetization of $YCrO_3$ along the crystallographic *b*-axis using a vibrating sample magnetometer in a zero field cool condition. Different pieces were used for specific heat and magnetization measurements, respectively.

2.2. Specific heat measurement scheme

To measure specific heat at low temperatures, we have replaced a sapphire platform in a commercial sample puck (PPMS^{TM}, Quantum Design) with our microcalorimeter as shown in Fig. 1(b). We have carefully measured the sample mass 55 μg with a micro-balance (SE2, Satorius). Before the measurement of specific heat, we have calibrated a sensor film made of ∼2000 Å thick Au and ∼30 Å thick Cr layers by measuring its resistance in a four-probe configuration. By regulating the temperature of the PPMS^{TM} cryostat in a high vacuum condition, we can control the temperature of the specific heat sample puck, *i.e.*, the reservoir temperature, to be constant. Then, an ac voltage output of a lock-in amplifier (SR830), V_C, is sent to an input of a current calibrator (Valhalla 2500) to generate ac currents applied to the sample, I_S, with a frequency ∼1 kHz. I_S is proportional to V_C, and is controlled automatically by software to vary from 10 to 100 μA. Then, the same lock-in amplifier measures V_S, *i.e.*, voltage generated across the thin film sensor to determine its resistance variation. Another thin film made of the Au/Cr layers is used as a heater. A source meter (Keithely 236) is turned on or off to apply dc current I_H while measuring dc voltage V_H generated across the film heater. A total power level, *i.e.*, $I_H V_H$ was adjusted to induce temperature increase less than ∼3% of the main reservoir temperature. We have developed a custom-made program based on LabVIEW^{TM} to control all of above instruments simultaneously; to set the block temperature, to measure the exponential variation of a sensor temperature with the heater turning-on or -off procedures, and to calculate heat capacity based on the CFM as explained below.

2.3. Application of the CFM to the microcalorimeter

The CFM considers a finite thermal conductance λ_s between the sample and the platform as well as a thermal conductance λ_l between the platform and the heat reservoir. Fig. 2(a) illustrates the relevant thermal parameters considered in the CFM. Detailed equations for the CFM are well documented by Hwang et al. [22]. Essentially, consideration of λ_s produces two relaxation times, τ_1 and τ_2:

$$T = A_1 \exp\left(\frac{-t}{\tau_1}\right) + A_2 \exp\left(\frac{-t}{\tau_2}\right) A_3 \quad (1)$$

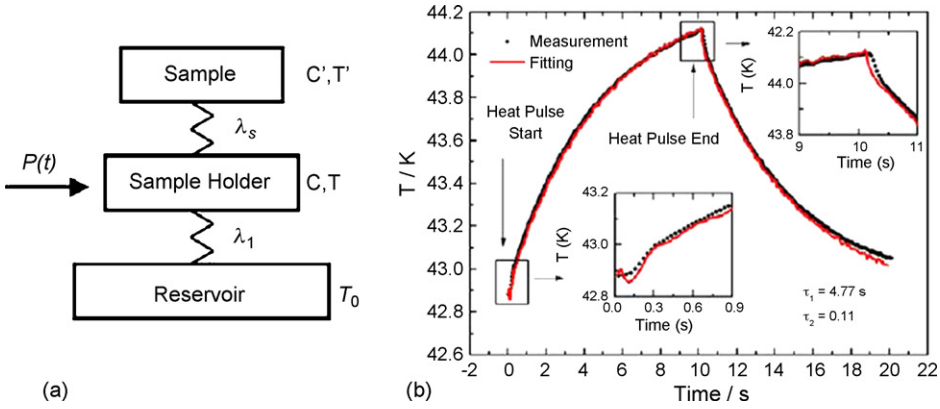

Fig. 2. (a) A schematic diagram of thermal parameters considered in the curve fitting method (CFM). $P(t)$ is the heat applied to the system. C and T are heat capacity and temperature of the sample holder, respectively. Prime denotes that of the sample contribution. λ_s represents a thermal conductance between the sample and the sample holder, while λ_1 means that between the sample holder and the heat reservoir. Heater current is turned on while the block temperature is fixed at T_0. (b) Variation of T per one measurement cycle with constant heater currents turned on or off. Turning-on and -off times of the current are indicated by two arrows. The blown-up inset shows a fast increase (drop) of temperature just after the heater current is turned-on (-off), which is caused by the presence of the τ_2 effect. The solid line refers to fits to the experimental data (solid circles) by use of the CFM, resulting in $\tau_1 = 4.77$ s and $\tau_2 = 0.11$ s.

Here, τ_1 and τ_2 can be expressed as a function of thermal parameters such as sample heat capacity C_s, addenda heat capacity $C_{addenda}$, λ_s and λ_1. In most of practical cases, τ_2 is not negligible so that it should be included to fit the temperature variation accurately. To get a reasonable fit of the experimental temperature variation, we have used a least square fitting method with three unknown constants given as functions of C_s, λ_s and λ_1 to fit the entire temperature response of the sensor film to the applied constant heater current [22]. On the other hand, $C_{addenda}$ is determined separately from the addenda measurement.

Fig. 2(b) illustrates the fitting results based on the CFM. After turning-on and -off time of heater currents, the temperature of the thin film sensor changes almost exponentially. However, as the inset shows, the measured decaying or increasing temperatures (solid circles) have very fast change driven by the short time constant τ_2, which is mainly due to the finite λ_s. The fit (solid line) based on the CFM results in $\tau_1 = 4.77$ s and $\tau_2 = 0.11$ s.

The CFM has several advantages over the conventional thermal relaxation method considering only a single relaxation time. First, it can estimate the τ_2 value as above. While the presence of an isothermal layer made of the Au film is partly useful to reduce the problem [15], the "τ_2 effect" is quite significant in the microcalorimeter measurement because one cannot press the sample easily on the membrane platform due to its fragility. Second, a total measurement time can be greatly reduced to $\sim$1–2τ, compared with a typical $\sim$10τ in the single relaxation time method.

3. Results and discussion

3.1. Specific heat and magnetic susceptibility data

Fig. 3 shows the heat capacity versus temperature (T) data from 30 to 360 K for the addenda without (solid triangle) and with (solid square) the $YCrO_3$ specimen with 55 μg. The addenda are composed of a Si–N membrane layer and a small amount of thermal grease. From typical measurement errors, the resolution of heat capacity is estimated to be as low as $\sim 10^{-6}$ J/K. It is found that the sample heat capacity shows the λ-shaped peak around $T_N \approx 140$ K, indicating a second order phase transition.

The peak, in fact, results from a canted AFM ordering of Cr^{3+} spins. It is well known that $RCrO_3$ compounds (R = Y and rare earths) show a weak ferromagnetism parasitic on the canted AFM. The canting of the staggered moment is driven by an anisotropic exchange due to Dzyaloshinsky–Moriya interaction [23]. Due to the canting of the staggered moment along b, magnetic susceptibility (χ) along b exhibits a weak ferromagnetic signal below $T_N \approx 140$ K and the corresponding $1/\chi$ shows a sharp decrease with decreasing T as in Fig. 3 (right axis). The heat capacity peak temperature matches with that of a maximum slope in $1/\chi$ versus T data. From a linear fit to the $1/\chi$ versus T plot above T_N, the Curie–Weiss temperature θ_{CW} is found to be $|\theta_{CW}| \approx 342$ K and the effective moment $\mu_{eff} \approx 3.8\mu_B$ per formula unit. θ_{CW} is rather higher than the actual $T_N \approx 140$ K by a factor of 2.44. Furthermore, $\mu_{eff} = 2\mu_B[S(S+1)]^{1/2} \approx 3.8\mu_B$

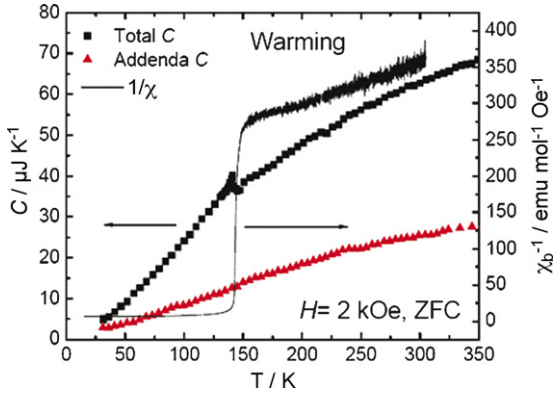

Fig. 3. The left axis summarizes heat capacity data of the microcalorimeter with (solid squares) and without (solid triangles) a single crystal $YCrO_3$ ($m = 55$ μg). Right axis shows the inverse magnetic susceptibility $1/\chi$ vs. T plot measured along b-axis at $H = 2$ kOe after zero field cooling. Both measurements indicate a canted antiferromagnetic ordering at $T_N \approx 140$ K.

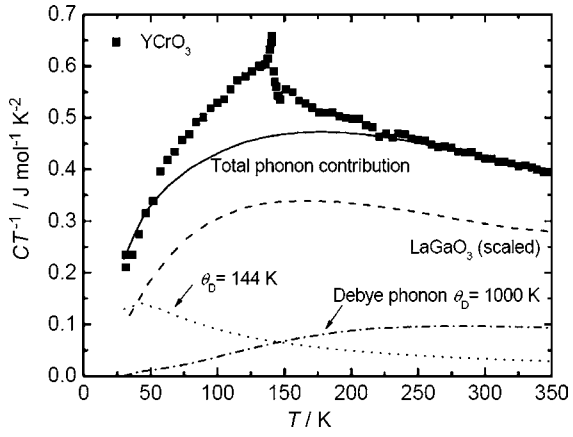

Fig. 4. The specific heat over temperature (C/T) data of $YCrO_3$ (solid squares) and $LaGaO_3$ (dashed line). The latter has been scaled by the Lindemann factor as explained in texts. Two additional phonon contributions, described by the Debye model with the Debye temperatures θ_D = 144 K (dotted line) and 1000 K (dashed-dotted line), were included to calculate the expected total phonon specific heat of $YCrO_3$ (solid line).

corresponds to $S \approx 1.46$ close to $S = 3/2$, a value expected from a Cr^{3+} ion subject to the orbital quenching effect in an octahedral crystal electric field.

3.2. Lindemann factor correction

Fig. 4 shows the resultant specific heat of $YCrO_3$ over temperature (C/T) calculated after subtracting the addenda heat capacity from the total one in Fig. 3. To extract the magnetic specific heat contribution of $YCrO_3$, we have initially assumed the phonon contribution of $YCrO_3$ is same as the C/T data of the non-magnetic analogue $LaGaO_3$ up to the Lindemann factor as explained below [24]. A similar C data of $LaGaO_3$ corrected by the Lindemann factor has been successfully used to estimate the phonon specific heat of $NdCrO_3$ [25]. Because mass and volume of $LaGaO_3$ are different from those of $YCrO_3$, an effective Debye temperature (θ_D) can be expressed as [26]:

$$\theta_D = L\left(\frac{T_m}{MV^{2/3}}\right)^{1/2} \quad (2)$$

where T_m is a melting temperature, M an atomic weight, and V an atomic volume. L is called as the Lindemann constant. Assuming that L and T_m are almost same for both $YCrO_3$ and $LaGaO_3$, θ_D of $YCrO_3$ is 1.197 times larger than that of $LaGaO_3$, due to the mass and volume difference. Thus, we can scale the temperature of the C versus T curve of $LaGaO_3$ by this Lindemann factor 1.197 to use as the estimated phonon C of $YCrO_3$. A dashed line in Fig. 3 shows the resultant C/T. This method relies on the assumption that both materials have almost the same Debye temperatures within a harmonic approximation up to the Lindemann factor [24]. It is noted that C of $LaGaO_3$ is best described by the Debye phonon model with three θ_Ds at 300, 350, and 900 K, respectively. A scaling of temperature by the Lindemann factor 1.197 means a scaling of all three θ_Ds by the same factor to calculate the phonon contribution of $YCrO_3$ by the Debye model.

With this estimation of the phonon C/T of $YCrO_3$, we have obtained the magnetic specific heat (C_{mag}) over T, C_{mag}/T, and also calculated the magnetic entropy (ΔS_{mag}) by integration of C_{mag}/T from 30 to 360 K. However, the resultant ΔS_{mag} versus T curve showed much larger values than the expected $\Delta S_{mag} = R\ln(2S+1) = 11.526\,J\,mol^{-1}\,K^{-1}$ (for $S = 3/2$) even well below T_N. Furthermore, it did not show any saturation to a finite value even at 360 K, much higher than T_N. Recalling that $S \approx 1.46$ of Cr^{3+} ions from the experimentally observed Curie–Weiss moment μ_{eff} is consistent with the expected $S = 3/2$, the observation of large excess entropy suggests existence of additional phonon entropy beyond the magnetic entropy of Cr^{3+} and the Lindemann factor corrected phonon entropy in a broad temperature region below and above T_N.

3.3. Additional phonon entropy and implication to ferroelectricity

To describe the C/T data in Fig. 4, we found that in addition to the C/T of $LaGaO_3$ with the Lindemann factor correction, at least were needed two more Debye phonon contributions with θ_D = 144 and 1000 K, respectively, as shown in dotted and dashed-dot lines. By including these two Debye model contributions, the remaining $\Delta S_{mag} \approx 13\,J\,mol^{-1}\,K^{-1}$ is found to be close to the expected one $11.54\,J\,mol^{-1}\,K^{-1}$, as shown in Fig. 5. The present results seem to be consistent with the fact that $YCrO_3$ is known to have the monoclinic structure with relatively low symmetry space group $P2_1/n$ (No. 14) in the literature [27] as compared with that of $LaGaO_3$, $Pbnm$ (No. 62) [28]. In other words, the additional Debye phonon modes of $YCrO_3$ might be a natural consequence of the monoclinic space group $P2_1/n$.

However, we note that $P2_1/n$ is still a centrosymmetric space group while the evidence of ferroelectricity seems to be experimentally convincing as observed by a dielectric constant peak and a ferroelectric hysteresis loop [11]. For the crystal investigated here, we have also found a broad dielectric constant peak around 500 K, as consistent with the reported $T_C \approx 473$ K of the polycrystalline $YCrO_3$ samples [11]. To explain these behaviors consistently, Serrao et al. have performed the spin-dependent

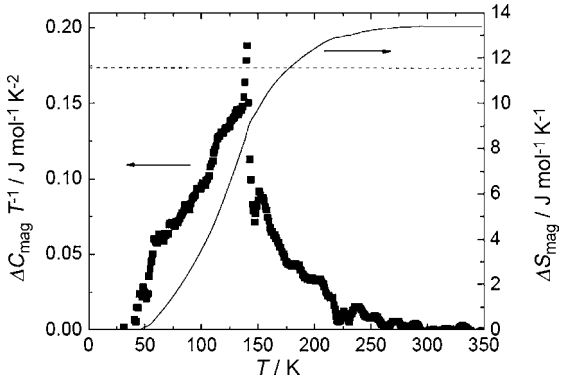

Fig. 5. Magnetic specific heat over temperature ($\Delta C_{mag}/T$) (left axis) of $YCrO_3$ (m = 55 μg) obtained after subtracting the phonon contribution (see texts for details). The solid line represents entropy (right axis) integrated with the $\Delta C_{mag}/T$ data. The dashed line marks the expected magnetic entropy of the Cr^{3+} ion with $S = 3/2$: $\Delta S_{mag} = R\ln(2S+1) = 11.53\,J\,mol^{-1}\,K^{-1}$.

density functional theory calculations to find out the final relaxed structure with the lowest energy has the broken inversion symmetry, of which space group is close to the monoclinic $P2_1$ (No. 4). From these results, we tentatively conclude that the additional Debye phonon modes could be related to the space group $P2_1$ rather than $P2_1/n$. In future, the actual space group of our crystal should be further investigated through the structural studies such as high resolution X-ray or neutron diffraction.

The present experimental results seem to be closely related to a comparative thermal conductivity study of $YCrO_3$ and $LaGaO_3$ by Zhou and Goodenough [29]. The phonon thermal conductivity of $YCrO_3$ is significantly suppressed overall temperatures below and above T_N as compared with that of $LaGaO_3$. Without information of the occurrence of ferroelectricity in $YCrO_3$ [11], Zhou and Goodenough [29] have attributed their results to the bond-length fluctuation of $YCrO_3$ coupled to the magnetic fluctuation above T_N that might come from an exchange striction driven by a strong spin–phonon coupling. Because the measured thermal conductivity is found to be much more suppressed even below T_N as well as above, however, the inhomogeneous bond-length fluctuation driven by magnetic fluctuation alone might not be enough to account for the experimental observation. If inversion symmetry-breaking phonon modes related to short ranged or long ranged ferroelectric dipoles exist below T_C and it gives the additional scattering of phonon thermal conductivity through the inhomogeneous bond-length fluctuation, one can expect both large excess entropy from the additional symmetry broken phonon modes and suppression of the phonon thermal conductivity overall temperatures. Therefore, all of these experimental observations coherently suggest that $YCrO_3$ has the additional phonon modes related to the monoclinic space group with an inversion symmetry breaking. In future, heat capacity studies of $YCrO_3$ up to temperatures above T_C, and direct measurements of phonon modes are desirable to further understand this compound.

4. Conclusion

We have measured the specific heat of a bi-ferroic $YCrO_3$ crystal with 55 μg using a high accuracy microcalorimeter between 30 and 360 K. $YCrO_3$ shows a sharp peak in the specific heat at $T_N \approx 140$ K due to a canted antiferromagnetic ordering. The analyses of magnetic and phononic entropy of $YCrO_3$ suggest that there exist additional phonon modes beyond those of $LaGaO_3$, which can be allowed in the monoclinic space group with a broken inversion symmetry below $T_C \approx 500$ K.

Acknowledgements

This work is supported by Korean Government through National Research Laboratory program (M10600000238), MOST and KRF (R08-2004-000-10228-0). KH is partially supported by KOSEF through CSCMR. KJW is supported by the Seoul R&BD and Seoul Science Fellowship.

References

[1] M. Fiebig, Th. Lottermoser, D. Frohlich, A.V. Goltsev, R.V. Pisarev, Nature (London) 419 (2002) 818.
[2] T. Kimura, T. Goto, H. Shintani, K. Ishizaka, T. Arima, Y. Tokura, Nature (London) 426 (2003) 55.
[3] N. Hur, S. Park, P.A. Sharma, J.S. Ahn, S. Guha, S.-W. Cheong, Nature (London) 429 (2004) 392.
[4] A. Moreira dos Santos, A.K. Cheetham, T. Atou, Y. Syono, Y. Yamaguchi, K. Ohoyama, H. Chiba, C.N.R. Rao, Phys. Rev. B 66 (2002) 064425.
[5] T. Kimura, S. Kawamoto, I. Yamada, M. Azuma, M. Takano, Y. Tokura, Phys. Rev. B 67 (2003) 18401(R).
[6] I. Sosnowska, T. Peterlin-Neumaier, E. Stiechele, J. Phys. C 15 (1982) 4835.
[7] S. Niitaka, M. Azuma, M. Takano, E. Nishibori, M. Takata, M. Sakata, Solid State Ionics 172 (2004) 557.
[8] R. Seshadri, N.A. Hill, Chem. Mater. 13 (2001) 2892.
[9] B.B. van Aken, T.T.M. Palstra, A. Filippetti, N.A. Spaldin, Nat. Mater. 3 (2004) 164.
[10] M. Kenzelmann, A.B. Harris, S. Jonas, C. Broholm, J. Schefer, S.B. Kim, C.L. Zhang, S.-W. Cheong, O.P. Vajk, J.W. Lynn, Phys. Rev. Lett. 95 (2005) 087206.
[11] C.R. Serrao, A.K. Kundu, S.B. Krupanodhi, U.V. Waghmare, C.N.R. Rao, Phys. Rev. B 72 (2005) 220101(R).
[12] A.K. Razdan, P.N. Kotru, B.M. Wanklyn, Mater. Sci. Eng. B 15 (1992) 199.
[13] K.S. Suh, H.J. Kim, Y.D. Park, K.H. Kim, J. Kor. Phys. Soc. 49 (2006) 1370–1378.
[14] S.G. Doettinger-Zech, M. Uhl, D.L. Sisson, A. Kapitulnik, Rev. Sci. Instrum. 72 (2001) 2398.
[15] D.W. Denlinger, E.N. Abarra, K. Allen, P.W. Rooney, M.T. Messer, S.K. Watson, F. Hellman, Rev. Sci. Instrum. 65 (1994) 946.
[16] S.L. Lai, G. Ramanath, L.H. Allen, P. Infante, Z. Ma, Appl. Phys. Lett. 67 (1995) 1229.
[17] Y.Y. Zhang, S. Tadigadapa, Appl. Phys. Lett. 86 (2005) 034101.
[18] E.A. Olson, M.Y. Efremov, A.T. Kwan, S. Lai, V. Petrova, F. Schiettekatte, J.T. Warren, M. Zhang, L.H. Allen, Appl. Phys. Lett. 77 (2000) 2671.
[19] M.Y. Efremov, E.A. Olson, M. Zhang, Z. Zhang, L.H. Allen, Phys. Rev. Lett. 91 (2003) 085703.
[20] S. Adamovsky, C. Schick, Thermochim. Acta 415 (2004) 1–7.
[21] Z.S. Zhang, O.M. Wilson, M.Y. Efremov, E.A. Olson, P.V. Braun, W. Senaratne, C.K. Ober, M. Zhang, L.H. Allen, Appl. Phys. Lett. 84 (2004) 5198.
[22] J.S. Hwang, K.J. Lin, C. Tien, Rev. Sci. Instrum. 68 (1997) 94.
[23] W.C. Koehler, E.O. Wollan, J. Phys. Chem. Solids 2 (1957) 100; W.C. Koehler, E.O. Wollan, M.K. Wilkinson, Phys. Rev. 118 (1960) 58.
[24] F. Lindemann, Z. Phys. 11 (1910) 609.
[25] F. Bartolome, J. Bartolome, Phys. Rev. B 62 (2000) 1058.
[26] A. Tari, The Specific Heat of Matter at Low Temperatures, Imperial College Press, 2003.
[27] L. Katz, Acta Crystallogr. 8 (1955) 121.
[28] D. Savytskii, L. Vasylechko, A. Senyshyn, A. Matkovskii, C. Bähtz, M.L. Sanjuán, U. Bismayer, M. Berkowski, Phys. Rev. B 68 (2003) 024101.
[29] J.-S. Zhou, J.B. Goodenough, Phys. Rev. B 66 (2002) 052401.